Hindawi
Journal of Electrical and Computer Engineering
Volume 2023, Article ID 5558246, 10 pages
https://doi.org/10.1155/2023/5558246

Research Article

Passivity-Based Control of Buck-Boost Converter for Different Loads Research

Feng Zhang,[1] Jianguo Li ,[2] Gejun Zhu,[1] Rongyuan Hu,[1] Yaping Qu,[3] and Yujiang Zhang[3]

[1]*State Nuclear Power Planning, Design and Research Institute Co., Ltd., Beijing, China*
[2]*School of Automation, Beijing Information Science and Technology University, Beijing, China*
[3]*Power Branch of Huomei Hongjun Aluminum Power Co., Ltd., Tongliao, Inner Mongolia Autonomous Region, China*

Correspondence should be addressed to Jianguo Li; lijianguo@bistu.edu.cn

Received 19 January 2023; Revised 5 May 2023; Accepted 3 June 2023; Published 9 June 2023

Academic Editor: Ramani Kannan

Normally, the buck-boost converter adopts single or double closed-loop control, and there are differences in control and parameters for different working modes and loads. In this study, a unified control method, the passivity-based control (PBC), is applied to a buck-boost converter for different loads, including constant resistance load (CRL), constant power load (CPL), and battery load. The PBC is a nonlinear control based on energy dissipation principle, and it has strong robustness to parameter interference and external disturbance, and it also has the advantages of simple design and simple implementation. Although many research studies have been conducted before, the voltage and current-related power losses are considered, and different load models are also compared in this research. The detailed mathematical model, control principle, and controller design of the buck-boost converter are thoroughly analysed. In addition, SIMULINK-based simulation results and experimental verification results of different loads are also given in the paper. Also, the PBC has smaller current overshot and smaller current ripples compared with PI control in different loads condition.

1. Introduction

A DC microgrid is usually composed of photovoltaic (PV) generator, battery energy storage system (BESS) and DC loads, and a PV generator; a BESS or a DC load requires either a higher or lower output voltage. To achieve a lower output voltage, a buck converter is used, and a boost converter is used when a higher output voltage is required. A buck-boost converter is used when a higher or lower DC output voltage is required at different times [1].

A buck-boost converter is either buck (lower) or boost (higher) converter, and it can transfer electrical energy bidirectionally. It has the advantages of simpler structure, lower cost, and higher reliability, and it is usually used to control the charging and discharging process in BESS, and a BESS converter is used to serve battery load [2].

Besides, when a PV converter is tightly regulated to stabilize the DC bus voltage, the DC bus will have a one-to-one voltage-current characteristic, and a PV converter is loaded with constant power load (CPL) [3]. Also, when a DC load has a constant resistance value, the DC load converter loads constant resistance load (CRL). In sum, the load of buck-boost converter may be battery load, CPL load, or CRL load, and different loads reveal different characteristics, so it is necessary to conduct the research of buck-boost converter in different loads condition.

The proportional integral differential control (PID) is most widely used in buck-boost converter to realize single closed-loop or double closed-loop control. It has the advantages of simple principle, easy implementation, and independence of system model [4, 5]. However, the buck-boost converter is a nonlinear time-varying system, and a PID cannot achieve the desired control effect, especially when the power source or load changes suddenly in a large range, and it even makes the converter unstable [6, 7].

To improve buck-boost converter's stability, some nonlinear controllers are developed and applied to the converter. In 1983, the sliding mode variable structure

control (SMVS) was first applied to DC/DC converter by Sabanovic et al. [8, 9]. After this, many improvements have been made to improve the converter's performance, such as elimination of variable switching frequency's influence, improvement of anti-interference capability, and reducing the natural buffeting. Despite all these improvements, SMVS has to determinate speed, inertia, acceleration, and switching surface parameters, and it is complex to implement online real-time control with a large amount of computation [10].

The adaptive control (APC) was also used in DC/DC converter [11–14]. The APC is a control method with online parameter identification, and it includes model reference adaptive control, self-tuning control, and parameter adaptive control. The APC also has strong robustness to parameter deviation and inaccurate model, but it is not widely used because of its serious lack of generality and openness. The optimization-based control was also used in DC/DC converter to attain the optimal droop resistances to minimize the error in the current sharing [15].

The neural network control (NNC) is the combination of neural network theory and control theory, and it is a control method by imitating biological neural system to process information. A NNC was also used in DC/DC converter to improve the transient performance of the converter. Although a NNC has the advantages of high nonlinear mapping capability, autonomous learning capacity, and fault tolerance capacity, it also has insufficient performance, such as low convergence speed, high sample dependence, and high initial network weight dependence [16, 17].

The passivity-based control (PBC), which was proposed by Ortega and Spong in 1989 [18], is a nonlinear control based on energy dissipation, and it utilizes energy dissipation to control stability and track given objects by means of damping injection. A PBC has the advantages of simple design and simple implementation, and it is already used in nonlinear system, such as motor control and power electronic devices. A PBC was also applied in DC/DC converter, and some measures have been made to eliminate steady-state error, which is caused by parasitic resistance, to improve the stability of CPL load [19–21]. However, the voltage and current-related loss are often ignored, and a unified PBC control strategy for different loads is not considered.

In the study, a unified PBC control strategy is applied to buck-boost converter, the voltage and current-related losses are considered independently, and battery load, CRL load, and CPL load are studied, respectively. Compared with previous research studies, the proposed control method is applied to different working modes and different loads, and it also has the advantages of simple design and simple implement. The buck-boost converter and different loads are analysed thoroughly, and the mathematical model in Euler–Lagrange (EL) form is deduced. In addition, the passivity characteristic is demonstrated, and a unified PBC controller is designed. Besides, the simulation and experimental verifications are carried out.

The rest of this study is organized as follows. In Section 2, the buck-boost topology is introduced and analysed thoroughly. In Section 3, the mathematical model based on EL equation is proposed. In Section 4, the unified PBC controller is designed according to the EL model. In Section 5, the different load models are given, Later in Sections 6 and 7, the results of simulation and experimental verification are given separately. Finally, Section 8 concludes the study.

2. Buck-Boost Converter Analysis

A buck-boost converter is made up of S_{d1}, S_{d2}, VD_1, VD_2, L_d, C_1, and C_2, as depicted in Figure 1. Here, S_{d1} and S_{d2} are all-controlling power switches, for example, MOSFET and IGBT. VD_1 and VD_2 are antiparallel power diodes. L_d is a DC inductor. R_1 and R_3 are used to simulate voltage-related loss, and R_2 is used to simulate current-related loss. A buck-boost converter can realize voltage conversion between different DC voltages, and it can exchange bidirectional power at the same time.

3. Buck-Boost Converter Mathematical Model

3.1. Buck State Model. When the power switch S_{d2} is turned off all the time and S_{d1} is controlled to turn on and off periodically, a buck converter is realized. Also, it converts constant voltage into variable voltage, such as charging the battery from DC bus.

In Figure 2, it shows the buck converter current path. When S_{d1} is turned on, the power diodes VD_1 and VD_2 are all turned off, and the current path is v_1-S_{d1}-L_d-R_2-v_2-v_1 as shown in Figure 2(a). At the time, the power supply v_1 transmits energy to the load v_2, while the inductor L_d stores energy, and the current i_2 increases.

When S_{d1} is turned off and the power diode VD_1 is also turned off, the current path is v_2-VD_2-L_d-R_2-v_2 as shown in Figure 2(b). At the time, the inductor L_d releases energy and transmits energy to the load v_2, and the current i_2 decreases.

According to Kirchhoff's voltage law, we can obtain

$$L_{\mathrm{d}}\frac{di_d}{dt} + R_2 i_{\mathrm{d}} + v_2 = D_1 v_1, \tag{1}$$

where D_1 is the duty ratio of power switch S_{d1}. D_1 is 0 when the switch is off, D_1 is 1 when the switch is on, and the duty ratio range is $0 \le D_1 \le 1$.

By writing the current equation for the output node, we can obtain

$$C_2\frac{dv_2}{dt} + \frac{v_2}{R_3} - i_d = -i_2. \tag{2}$$

Synthesizing (1) and (2),

$$\begin{cases} L_d\dfrac{di_d}{dt} + R_2 i_d + v_2 = D_1 v_1, \\ \\ C_2\dfrac{dv_2}{dt} + \dfrac{v_2}{R_3} - i_d = -i_2, \end{cases} \tag{3}$$

where I_1 and I_2 are mean currents of input and output, respectively.

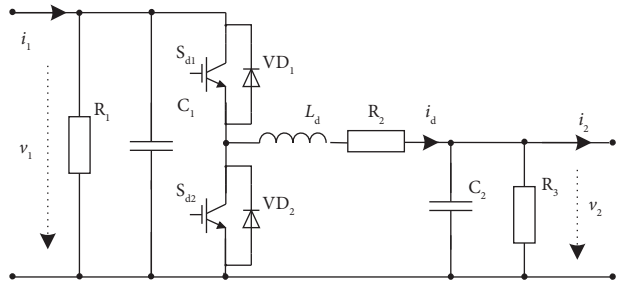

Figure 1: The buck-boost converter topology.

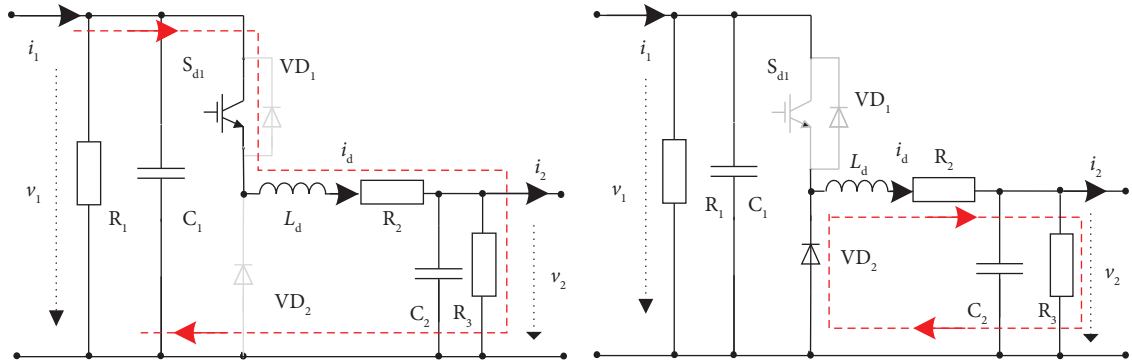

Figure 2: Buck state current analysis. (a) S_{d1} turns on and (b) S_{d1} turns off.

3.2. Boost State Model. When the power switch S_{d1} is turned off all the time and S_{d2} is controlled to turn on and off periodically, a boost converter is realized. Also, it converts variable voltage into constant voltage, such as discharging the battery to DC bus.

In Figure 3, it shows the boost converter current path. When S_{d2} is turned on and the power diodes VD_1 and VD_2 are all turned off, the current path is $v_2 - R_2 - L_d - S_{d2} - v_2$ as shown in Figure 3(a). Compared with Figure 2(b), the current flows S_{d2} in the opposite direction. At the time, the power supply v_2 stores energy in the inductor L_d, and the current i_2 increases, which also meets (2).

When S_{d2} is turned off and the power diode VD_2 is turned off, the current path is $v_2 - R_2 - L_d - VD_1 - v_1 - v_2$ as shown in Figure 3(b). Compared with Figure 2(a), the current flows VD_1 in the opposite direction. At the time, the power supply v_2 transmits energy to the microgrid v_1, the inductor L_d releases energy, and the current i_2 decreases, which also meets (1).

If the duty ratio of the power switch S_{d2} is set as D_2, D_2 is 0 when the switch is off, D_2 is 1 when the switch is on, and the duty ratio range is $0 \le D_2 \le 1$.

The buck-boost converter can be expressed as follows:

$$\begin{cases} L_d \dfrac{di_d}{dt} + R_2 i_d + v_2 = D_1 v_1, \\ C_2 \dfrac{dv_2}{dt} + \dfrac{v_2}{R_3} - i_d = -i_2, \\ D_2 = 1 - D_1. \end{cases} \tag{4}$$

If the state variable is $\mathbf{X} = (i_d, v_2)^T$ and the input variable is $\mathbf{V} = (D_1 v_1, -i_2)^T$, (4) can be sorted into Euler equation in the form of

$$\mathbf{M}\dot{\mathbf{X}} + \mathbf{J}\mathbf{X} + \mathbf{R}\mathbf{X} = \mathbf{V}, \tag{5}$$

where $\mathbf{M}$ is a positive definite symmetric coefficient matrix, i.e., $\mathbf{M}^T = \mathbf{M}$. $\mathbf{J}$ is an antisymmetric coefficient matrix, i.e., $\mathbf{J}^T = -\mathbf{J}$. $\mathbf{R}$ is a positive coefficient matrix, i.e., $\mathbf{R}^T = \mathbf{R} > 0$, which means that the converter has dissipative characteristic.

$$\mathbf{M} = \begin{pmatrix} L_d & 0 \\ 0 & C_2 \end{pmatrix}, \mathbf{J} = \begin{pmatrix} 0 & 1 \\ -1 & 0 \end{pmatrix}, \mathbf{R} = \begin{pmatrix} R_2 & 0 \\ 0 & \dfrac{1}{R_3} \end{pmatrix}. \tag{6}$$

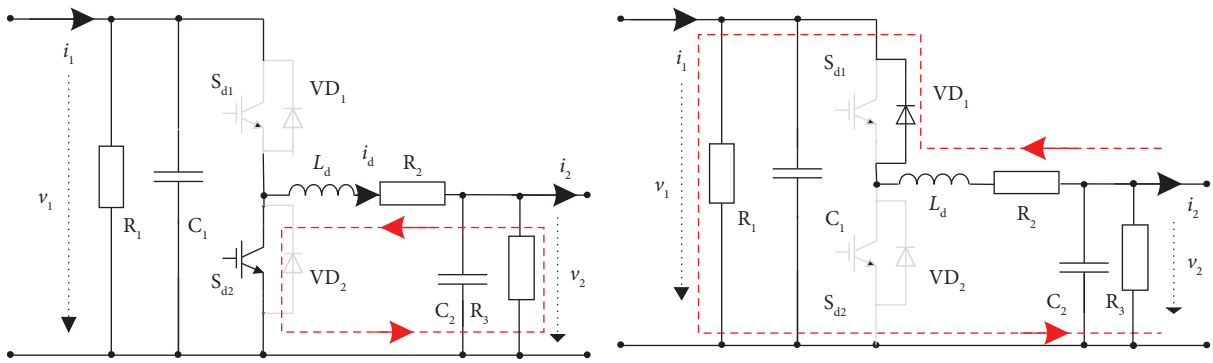

Figure 3: Boost state current analysis. (a) S_{d2} turns on and (b) S_{d2} turns off.

4. Passivity-Based Controller Design

It is assumed that the target values of state variables are i_d^* and v_2^*, respectively, that is, $\mathbf{X}^* = (i_d^*, v_2^*)^T$, and the error variable is $\mathbf{X}_e = \mathbf{X} - \mathbf{X}^*$; according to (5), we can obtain

$$\begin{aligned}\mathbf{M}\dot{\mathbf{X}}_e + \mathbf{J}\mathbf{X}_e + \mathbf{R}\mathbf{X}_e &= \mathbf{M}\left(\dot{\mathbf{X}} - \dot{\mathbf{X}}^*\right) + \mathbf{J}\left(\mathbf{X} - \mathbf{X}^*\right) \\ &\quad + \mathbf{R}\left(\mathbf{X} - \mathbf{X}^*\right) \\ &= \mathbf{M}\dot{\mathbf{X}} + \mathbf{J}\mathbf{X} + \mathbf{R}\mathbf{X} - \left(\mathbf{M}\dot{\mathbf{X}}^* + \mathbf{J}\mathbf{X}^* + \mathbf{R}\mathbf{X}^*\right) \\ &= \mathbf{V} - \left(\mathbf{M}\dot{\mathbf{X}}^* + \mathbf{J}\mathbf{X}^* + \mathbf{R}\mathbf{X}^*\right).\end{aligned} \tag{7}$$

To accelerate the convergence rate of $\mathbf{X}_e$ to 0, a damping coefficient matrix $\mathbf{R}_d = \mathrm{diag}\{r_{11}, g_{22}\}$ is used to accelerate $\mathbf{X}$ approach to $\mathbf{X}^*$; therefore, it can be rewritten as follows:

$$\mathbf{M}\dot{\mathbf{X}}_e + \mathbf{J}\mathbf{X}_e + (\mathbf{R} + \mathbf{R}_d)\mathbf{X}_e = \mathbf{V} - \left(\mathbf{M}\dot{\mathbf{X}}^* + \mathbf{J}\mathbf{X}^* + \mathbf{R}\mathbf{X}^* - \mathbf{R}_d\mathbf{X}_e\right), \tag{8}$$

where r_{11} and g_{22} are the injection damping coefficients.

According to the theory of PBC [19], the PBC controller can be designed as follows:

$$\mathbf{V} = \mathbf{M}\dot{\mathbf{X}}^* + \mathbf{J}\mathbf{X}^* + \mathbf{R}\mathbf{X}^* - \mathbf{R}_d\mathbf{X}_e. \tag{9}$$

The matrix equation can be further expressed as the following differential equation form:

$$\begin{cases} D_1 v_1 = L_d \dfrac{di_d^*}{dt} + v_2^* + R_2 i_d^* - r_{11}\left(i_d - i_d^*\right), \\ -i_2 = C_2 \dfrac{dv_2^*}{dt} - i_d^* + \dfrac{v_2^*}{R_3} - g_{22}\left(v_2 - v_2^*\right). \end{cases} \tag{10}$$

4.1. Constant Current Control. When a buck-boost converter works in constant current control (CCC) mode, the reference i_d^* is used as control target. So the first control equation with i_d^* is selected, and v_2^* is replaced by the sampling voltage v_2. So, we can obtain

$$D_1 = \frac{v_2 + L_d\left(di_d^*/dt\right) + R_2 i_d^* - r_{11}\left(i_d - i_d^*\right)}{v_1}. \tag{11}$$

4.2. Constant Voltage Control. When a buck-boost converter works in constant voltage control (CVC) mode, the current reference i_d^* and voltage reference v_2^* are all used as control target. So, we can obtain

$$D_1 = \frac{v_2^* + L_d\left(di_d^*/dt\right) + R_2 i_d^* - r_{11}\left(i_d - i_d^*\right)}{v_1}. \tag{12}$$

Normally, the voltage reference is manually set directly, and the current reference is gotten by a PI controller indirectly in the CVC mode, that is,

$$i_d^* = \left(k_p + \frac{k_i}{s}\right)\left(v_2^* - v_2\right), \tag{13}$$

where k_p and k_i are proportional and integral coefficients, respectively.

The current response is derived as follows:

$$i_d = i_d^* + A_d e^{-(t/\tau)}, \tag{14}$$

where A_d is the initial values of transient components and τ is the time constant.

$$\tau = \frac{L_d}{R_2 + r_{11}}. \tag{15}$$

It implies that when τ is greater than 0, i_d converges to i_d^*. Also, when r_{11} is larger, the convergence speed is faster, and current transfer function is

$$G(s) = \frac{1 - T_s s/2}{(\tau s + 1)\left(1 + T_s s/2\right)}, \tag{16}$$

where T_s is the sampling delay time. According to control theory, when $\mathrm{Re}|G(j\omega)|$ is greater than 0, the system is internally stable, so we can get the range of damping coefficient r_{11}.

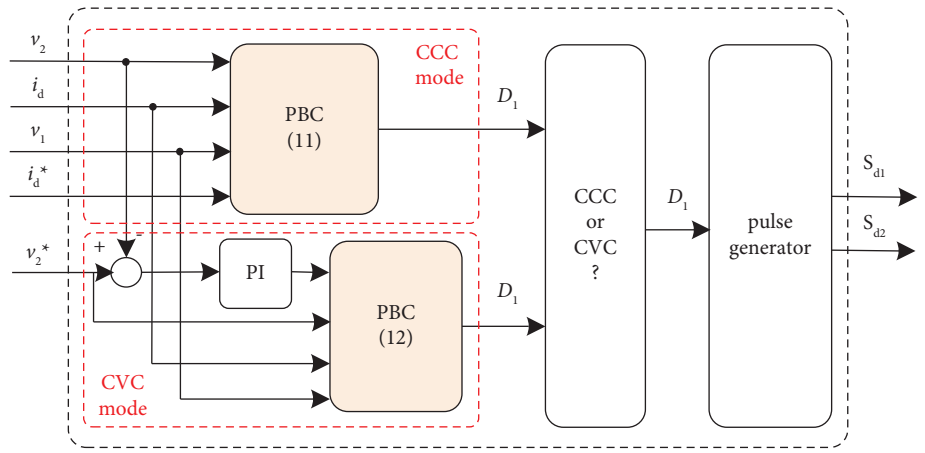

Figure 4: The PBC control diagram of the buck-boost converter.

$$r_{11} > \frac{4\omega^2 L_d T_s}{4 - \omega^2 T_s^2} - R_2. \tag{17}$$

Figure 4 shows the buck-boost converter's control diagram. When a buck-boost converter supplies CRL loads or CPL loads, the CVC mode is usually used. Also, when a buck-boost converter supplies battery loads, the CCC mode and CVC modes are used according to the state of charge (SOC) of the battery.

It can be seen that only L_d is used in the controller, and it only affects the derivative of current reference (di_d^*/dt). The current reference usually comes from a PI controller, and its output has a relatively large range, so the parametric uncertainty of L_d has almost no significant impact on the system. In addition, the load current i_d only appears in the damping term, and the load disturbance also has no significant impact on the system. The PBC has inherent strong robustness against parametric uncertainties and load disturbances.

5. Different Loads Model

5.1. Constant Power Load Model. A CPL consumes constant power within a certain voltage range, and the voltage and current can be expressed as follows:

$$v_2 i_2 = P, \tag{18}$$

where P is the constant power, and its incremental resistance is negative, which means that the current drawn by the load increases or decreases with the decrease or increase of voltage, that is

$$R_{\mathrm{CPL}} = \left.\frac{dv_2}{di_2}\right|_{v_2 = V_2} = -\frac{V_2^2}{P}. \tag{19}$$

The voltage and current characteristic of the CPL, which is shown in Figure 5(a), can be expressed as follows [19]:

$$i_2 = -\frac{P}{V_2^2} v_2 + \frac{2P}{V_2}, \tag{20}$$

where V_2 is steady state voltage, and CPL can be equivalent to the parallel connection of a controlled current source and a negative resistor, as shown in Figure 5(b).

5.2. Battery Load Model. The battery can be equivalent to a variable voltage source with a variable internal resistance, and the variable equivalent voltage is related to the battery's state of charge (SOC), and the variable internal resistance is related to battery's ohmic resistance and polarization resistance. The ohmic resistance is constant for a particular battery, but the polarization resistance changes all the time according to the battery's working conditions. Figure 6 gives the battery's equivalent circuit, and it can be expressed as follows:

$$\begin{cases} v_2 = E_0 + i_2 (R_0 + R_r), \\ R_r C_r \dfrac{di_r}{dt} = i_2 - i_r. \end{cases} \tag{21}$$

6. Simulation Verification

To validate the superiority of PBC over PI in different loads, simulations based on SIMULINK are carried out. The main circuit parameters of the buck-boost converter are shown in Table 1, and the control coefficients are listed in Table 2.

6.1. Battery Load Simulation. In Figure 7, it shows the current waveforms compared with PI control with battery load. At the time $t = 0$, the buck-boost converter starts to go to CCC mode with 20 A charging current reference, then go to CVC mode with 705 V charging voltage reference at the time t_1, finally go to CCD mode with −20 A discharging current reference at the time t_2. Whatever with PI control or PBC control, the buck-boost converter tracks the control command quickly.

Compared with PI control, the PBC control has no obvious current overshot in the transient processes, and it also has smaller current ripples in the steady state. Also, it shows that PBC has better transient and steady characteristics in battery load condition.

6.2. Constant Power Load Simulation. In Figure 8, it shows the current waveforms compared with PI control with CPL load. At the time $t = 0$, the buck-boost converter supplies

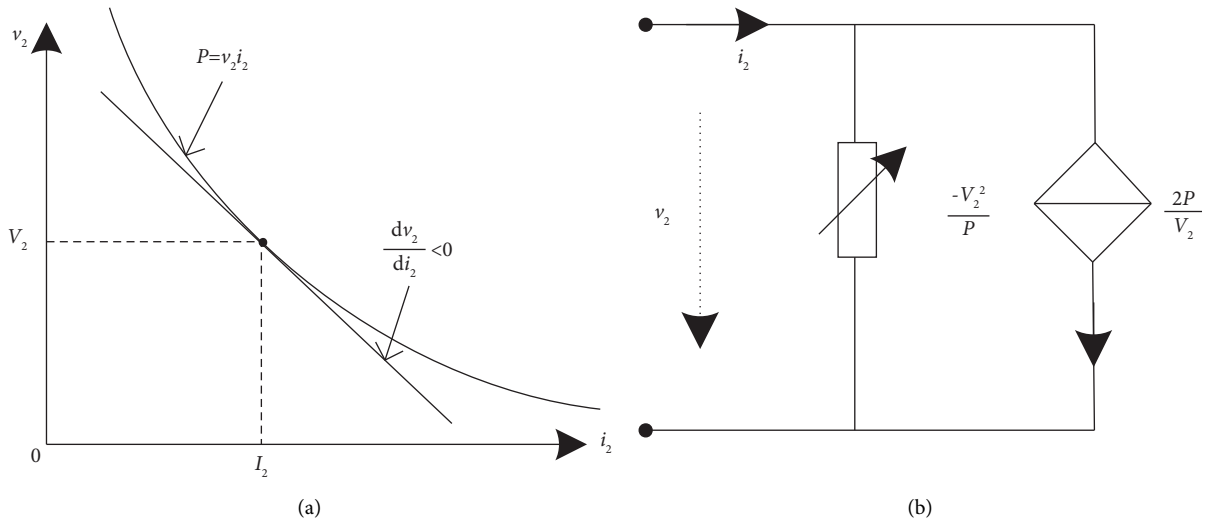

Figure 5: CPL characteristic: (a) voltage and current characteristic and (b) equivalent circuit.

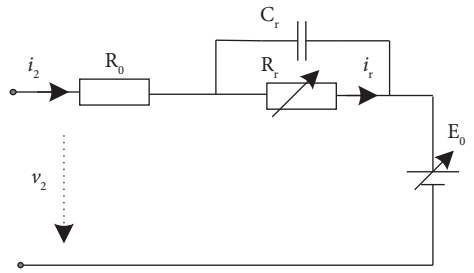

Figure 6: The battery equivalent circuit.

Table 1: Main circuit parameters of buck-boost converter.

Parameters	Value
Supply voltage v_1 (V)	750
Capacitor C_1 (μF)	1100
Equivalent resistor R_1 (kΩ)	100
Capacitor C_2 (μF)	470
Equivalent resistor R_2 (Ω)	0.5
Inductor L_d (mH)	10.0
Battery rated voltage v_2 (V)	700
Battery equivalent resistor (Ω)	0.5
Equivalent resistor R_3 (kΩ)	100

Table 2: Control coefficients of buck-boost rectifier.

Coefficients	Value
Switching frequency (kHz)	100
Passive damping coefficient r_{11}	800
Proportional coefficient k_p	0.2
Integral coefficient k_i	5

10 kW rated CPL load, the CPL load increases to 15 kW at the time t_3, then the supplied voltage is reduced to 600 V at the time t_4, after that the CPL load decreases to 10 kW at the time t_5, finally the supplied voltage is restored to 705 V at the time t_6. Whatever with PI control or PBC control, the buck-boost converter works well to response the control command.

Compared with PI control, the PBC control has smaller current ripples, which has been reduced by 67.23%, throughout the process. And, it shows that the PBC control has better characteristics over PI control in CPL load condition.

6.3. Constant Resistance Load Simulation. In Figure 9, it shows the current waveforms compared with PI control with CRL load. At the time $t = 0$, the buck-boost converter supplies 70 Ω resistance load, another 70 Ω resistance is connected at the time t_7, then the supplied voltage is reduced to 600 V at the time t_8, finally the supplied voltage is restored to 705 V at the time t_9.

Compared with PI control, the PBC control has smaller transient current overshot, which has been reduced by 14.29%, and it also has smaller current ripples in steady state. And, it shows that a PBC control has better transient and steady state characteristics over PI control in CRL load condition.

Through the simulation comparation of buck-boost converter with battery load, CPL load, and CRL load, the PBC control has smaller current overshot and smaller current ripples, and it has better transient and steady state characteristics over PI control.

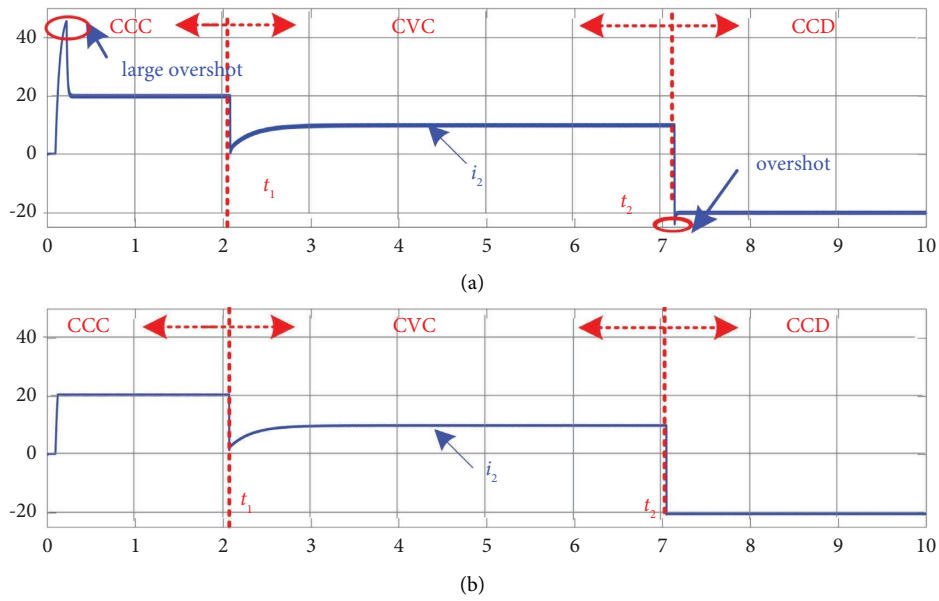

Figure 7: Current waveforms comparation in battery load simulation. (a) PI control. (b) PBC control.

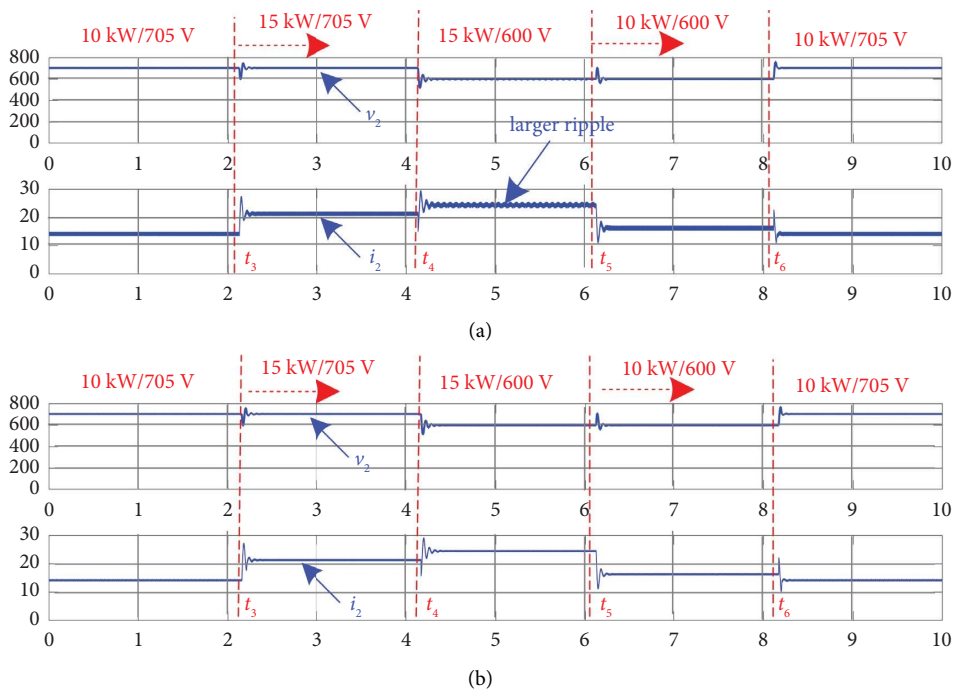

Figure 8: Current waveforms comparison in CPL simulation. (a) PI control. (b) PBC control.

7. Experimental Verification

To further verify the PBC control of buck-boost converter with different loads, a downsize buck-boost converter is built, and a bidirectional DC power of PSB9750-20 (Elektro Automatik company) is used as power supply, an electronic load of MWBPF2-1040 (MyWay company) is used as CPL load and CRL load, and 4 lead-acid battery cells are used as battery load, as shown in Figure 10.

7.1. Battery Load Verification. In Figure 11, it shows experimental waveforms with battery load. The input voltage is 50 V, and the buck-boost converter works in constant current state with battery load. At the time t_1, the buck-boost converter starts to change from CCC state to CCD state, the current changes from 1 A to −1 A, and the voltage changes from 44 V to 32 V. At the time t_2, the reverse change process from CCD state to CCC state occurs. The dynamic response time is less than 10 ms, and there is no current overshot

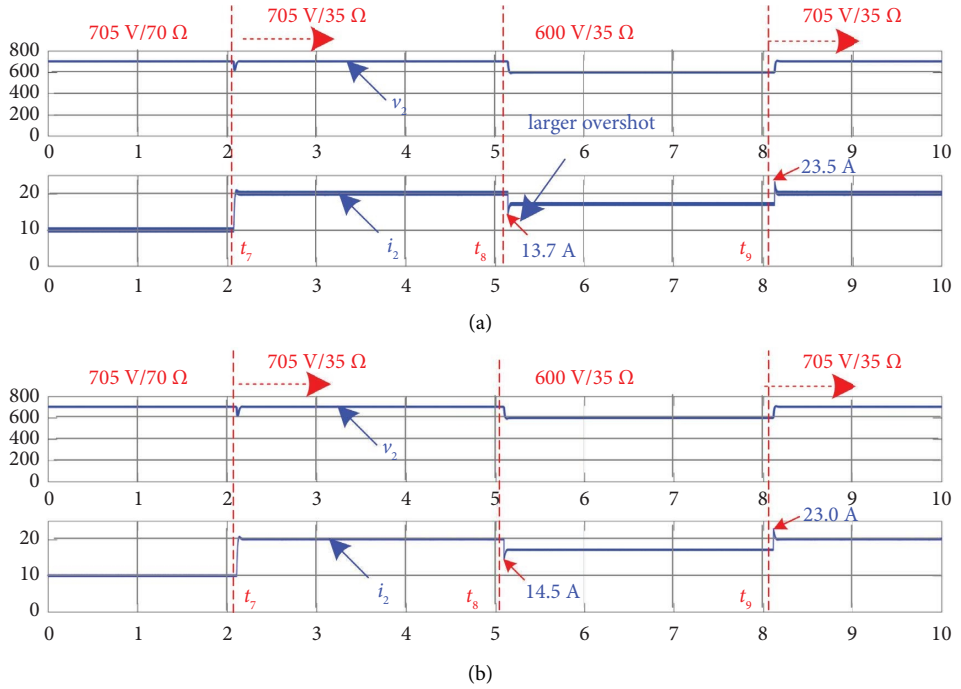

Figure 9: Current waveforms comparation in CRL load simulation. (a) PI control. (b) PBC control.

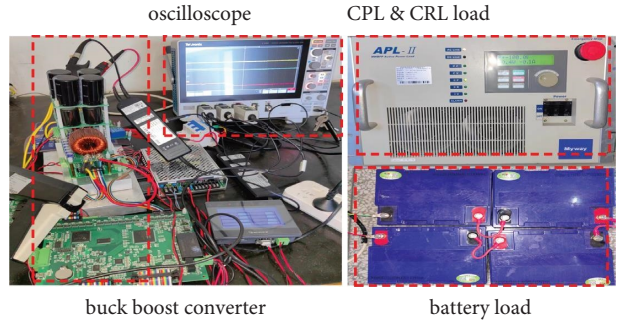

Figure 10: The buck-boost converter prototype.

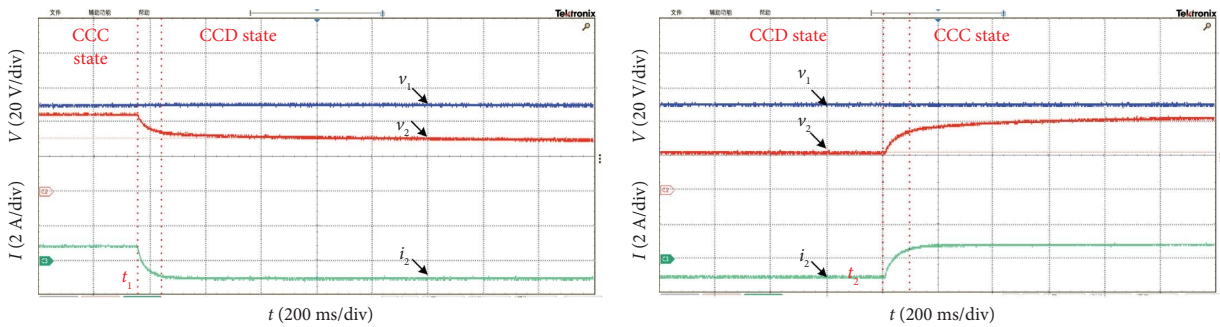

Figure 11: Experimental waveforms with battery load. (a) CCC to CCD state. (b) CCD to CCC state.

during transient processes. Because of its high internal resistance, the battery voltage has also undergone a larger change.

7.2. Constant Power Load Verification. In Figure 12, it shows experimental waveforms with CPL load. The input voltage is 50 V, and the buck-boost converter works with CPL load of

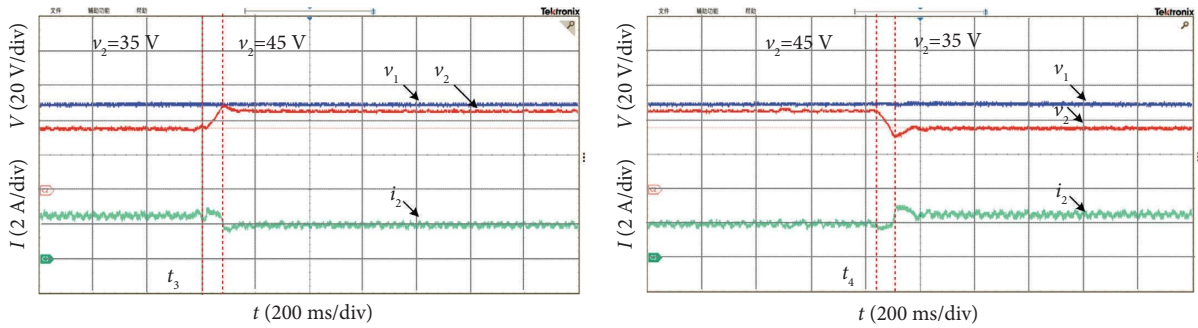

Figure 12: Experimental waveforms with CPL load. (a) Voltage reference from 35 V to 45 V. (b) Voltage reference from 45 V to 35 V.

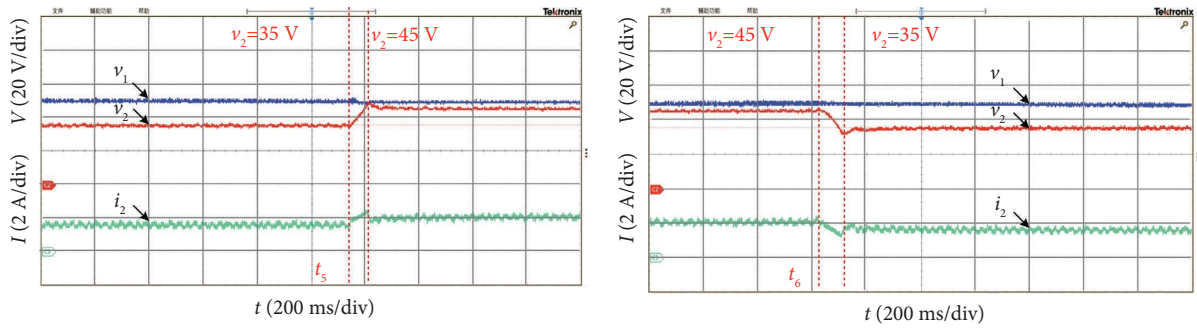

Figure 13: Experimental waveforms with CRL load. (a) Voltage reference from 35 V to 45 V. (b) Voltage reference from 45 V to 35 V.

100 W. At the time t_3, the buck-boost converter starts to change voltage reference from 35 V to 45 V, the voltage tracks the command quickly, and the current decreases from 2.7 A to 2.0 A accordingly. At the time t_4, the reverse voltage reference change process from 45 V to 35 V occurs. The dynamic response time is less than 8 ms, and there is also no current overshot during transient processes.

7.3. Constant Resistance Load Verification. In Figure 13, it shows experimental waveforms with CRL load. The input voltage is 50 V, and the buck-boost converter works with CRL load of 20 Ω. At the time t_5, the buck-boost converter starts to change voltage reference from 35 V to 45 V, the voltage tracks the command quickly, and the current increases from 1.7 A to 2.0 A accordingly. At the time t_6, the reverse voltage reference change process from 45 V to 35 V occurs. The dynamic response time is also less than 8 ms, and there is also no current overshot during transient processes.

Through the experimental verifications, the PBC control of buck-boost converter has better transient and steady state characteristics whatever in battery load or in CPL load and CRL load.

8. Conclusion

A buck-boost converter is often used in DC microgrid, and it loads battery load, CPL load or CRL load when it connects BESS, PV, and DC loads. In the study, a unified PBC control is applied to buck-boost converter with different loads. Some theoretical analysis, simulation, and experimental verifications have been conducted in the study.

The results show that compared with PI control, the PBC control has smaller current overshot, which has been reduced by 14.29%, and it has smaller current ripples, which has been reduced more than 50% with CPL load. The PBC control has better transient and steady state characteristics over PI control.

Besides, the unified PBC control is applied to different working modes and different loads, and it also has the advantages of simple design and simple implement. It has strong robustness because of its energy control principle, but it does not handle small signal and large signal disturbances separately.

Although some experimental researches have been conducted, more comparison of different control methods and more in-depth research studies still need to be strengthened. In addition, the research of parametric uncertainty verification will be further conducted in the following research.

Data Availability

The data used to support the study are openly available in a public repository.

Conflicts of Interest

The authors declare that they have no conflicts of interest.

Acknowledgments

The authors give their sincere appreciations to the support of Class B1 Key Scientific Research Projects of State Power Investment Group (Grant no. KYB12022ZH01) and State Natural Science Foundation Program of China (Grant no. 52107176).

References

[1] R. Kaye and A. Kalam, "Non-isolated DC/DC buck/boost converters for off-grid hybrid renewable system," in *Proceedings of the 2019 29th Australasian Universities Power Engineering Conference (AUPEC)*, pp. 1–5, November 2019, Nadi, Fiji.

[2] J. Chen, Y. Liu, and G. Bao, "Optimal operating strategy for distribution networks with PV and BESS considering flexible energy storage," in *Proceedings of the IEEE power and energy society general meeting (PESGM)*, pp. 1–5, Boston, MA, USA, November 2016.

[3] C. Zhang, G. Buticchi, J. Yang, and Z. Zou, "Control and stabilization of grid-connected converters operating as constant power load in a smart transformer grid scenario," in *Proceedings of the 46th Annual Conference of the IEEE Industrial Electronics Society*, pp. 2895–2900, Singapore, October 2020.

[4] N. Tiwari and A. N. Tiwari, "Performance analysis of unidirectional and bidirectional buck-boost converter using PID controller," in *Proceedings of the International Conference on Electronics, Materials Engineering & Nano-Technology (IEMENTech)*, pp. 1–6, Kolkata, India, September 2018.

[5] K. Ramireddy, Y. Hirpara, and Y. V. Pavan Kumar, "Transient performance analysis of buck boost converter using various PID gain tuning methods," in *Proceedings of the International Conference on Computational Intelligence and Communication Networks (CICN)*, pp. 321–326, Bhimtal, India, November 2020.

[6] L. Chen, J. Xu, S. Cheng, L. Liu, and L. Deng, "Stability analysis and AC modeling of high-efficiency BUCK/BOOST converter," in *Proceedings of the IEEE International Conference on Electron Devices and Solid-State Circuits*, pp. 1–4, Hong Kong, China, January 2008.

[7] M. Veerachary and M. R. Khuntia, "Design and Analysis of two-switch-based enhanced gain buck–boost converters," *IEEE Transactions on Industrial Electronics*, vol. 69, no. 4, pp. 3577–3587, 2022.

[8] A. Sabanovic and F. Bilalovic, "Sliding mode control of AC drives," *IEEE Transactions on Industry Applications*, vol. 25, no. 1, pp. 70–75, 1989.

[9] S. Tan, Y. Lai, C. Tse, and M. Cheung, "A fixed-frequency pulse width modulation based quasi-sliding-mode controller for buck converters," *IEEE Transactions on Power Electronics*, vol. 20, no. 6, pp. 1379–1392, 2005.

[10] O. Lopez, L. Garcia De Vicuna, M. Castilla, J. Matas, and M. Lopez, "Sliding-mode-control design of a high-power-factorbuck-boost rectifier," *IEEE Transactions on Industrial Electronics*, vol. 46, no. 3, pp. 604–612, 1999.

[11] W. Hu and D. Zhou, "Adaptive control of DC-DC converters based on input equivalent disturbance," in *Proceedings of the Chinese Control Conference*, pp. 38–42, Kunming, China, August 2008.

[12] S. Kasicheyanula and V. John, "Adaptive control strategy for ultracapacitor based bidirectional DC–DC converters," *IEEE Transactions on Industry Applications*, vol. 55, no. 2, pp. 1717–1728, 2019.

[13] W. Hatahet, M. I. Marei, and M. Mokhtar, "Adaptive controllers for grid-connected DC microgrids," *International Journal of Electrical Power & Energy Systems*, vol. 130, pp. 106917–106924, 2021.

[14] S. Mohamed, M. Mokhtar, and M. Marei, "An adaptive control of remote hybrid microgrid based on the CMPN algorithm," *Electric Power Systems Research*, vol. 213, pp. 108793–108806, 2022.

[15] M. Mokhtar, M. Marei, and A. A. El-Sattar, "Improved current sharing techniques for DC microgrids," *Electric Power Components and Systems*, vol. 46, no. 7, pp. 757–767, 2018.

[16] F. Kurokawa, H. Maruta, T. Mizoguchi, A. Nakamura, and H. Osuga, "A new digital control DC-DC converter with multi-layer neural network predictor," in *Proceedings of the International Conference on Machine Learning and Applications*, pp. 638–643, Miami, USA, December 2009.

[17] H. Maruta, M. Motomura, and F. Kurokawa, "A novel neural network based control method with adaptive on-line training for DC-DC converters," in *Proceedings of the International Conference on Machine Learning and Applications*, pp. 503–508, Boca Raton, FL, USA, December 2012.

[18] R. Ortega and M. Spong, "Adaptive motion control of rigid robots: a tutorial," *Automatica*, vol. 25, no. 6, pp. 877–888, 1989.

[19] M. Wang, F. Tang, X. Wu, Y. Zhang, and J. Wang, "Passivation and passivity-based control of DC–DC converter with unknown constant power loads," *IEEE Journal of Emerging and Selected Topics in Power Electronics*, vol. 10, no. 4, pp. 4041–4058, 2022.

[20] E. Hernández-Márquez, R. Silva-Ortigoza, J. García-Sánchez, M. Marcelino-Aranda, and G. Saldaña-González, "A DC/DC buck-boost converter–inverter–DC motor system: sensorless passivity-based control," *IEEE Access*, vol. 6, pp. 31486–31492, 2018.

[21] S. Pang, B. Nahid-Mobarakeh, S. Pierfederici, Y. Huangfu, G. Luo, and F. Gao, "Large-signal stable nonlinear control of DC/DC power converter with online estimation of uncertainties," *IEEE Journal of Emerging and Selected Topics in Power Electronics*, vol. 9, no. 6, pp. 7355–7368, 2021.